Proceedings World Geothermal Congress 2020+1
Reykjavik, Iceland, April - October 2021

Geochemical Characteristics of Fluids from Northwest Algeria

Mohamed Belhai, Yasuhiro Fujimitsu, Rosa Maria Barragan-Reyes, Tatsuto Iwanaga, Mamiko Maeno, Brahim Ayad, Fatima Zohra Bouchareb-Haouchine, Jun Nishijima, Djelloul Belhai, Abdelhamid Haouchine

Mohamed.Belhai@sunnyhillenergy.com, mkhader89@gmail.com

Keywords: Algeria, non-volcanogenic, thermal waters, gas mixing models, deeply infiltrated, geothermometers.

ABSTRACT

Geothermal manifestations of thermal springs, travertine deposition and hydrothermal alteration zones in the Northwestern part of Algeria were formed during the Mio-Plio-Quaternary volcanic activities. The geothermal reservoirs are hosted in the fractured Jurassic dolomite and limestone formations, named the "Tlemcenian dolomites formations". The chemistry of twenty-one hot spring water samples highlights the heterogeneity of water mineralization processes in NW Algeria. Three major types of water were identified: Na-Cl, Ca-SO_4 and Na-HCO_3 (Cl). The first two water types contain high salinity and higher contents of F, B, Li, Br and Cs, and are derived from evaporites rich in halite and gypsum minerals, linked to the Triassic extrusion and Messinian saline formation of the Atlasic land and the Tellian sector, respectively. While the third type is mainly associated with the carbonate forma tions of the Tellian sector. The stable isotopes (δ^{18} O and δ2H) results and the gas mixing models (N_2-He*1000-Ar*100 with O_2-CO_2-He*1000) reveal the meteoric origin of the thermal waters. According to the Na-K-Mg Ternary plot, the thermal waters are immature. The deep geothermal reservoir temperatures are presumed to be circa 140°C based on K/Na Giggenbach geothermometer model. The geochemical conceptual model indicates the meteoric origin of thermal springs which were heated as result of deep infiltration and conductive heat flow (120 mW/m^2) in the region brought about by tectonic activity. The deep geothermal fluids are mixed with cooler waters rich in Mg and leach Mg from the surrounding rocks during their rise to the surface.

1. INTRODUCTION

Northern Algeria is part of the Alpine-Maghrebide belt orogeny which resulted from the active collision of European continental plate with the African margin which started in the late Permian and ended up in the upper Miocene. This complex tectonic evolution has generated recent Mio-Plio-Quaternary volcanism, vigorous seismic activity and has led to the emergence of more than 120 hot springs spread along the Maghrebide belt for about 1200 km in the northern part of Algeria. Furthermore, the number and location of these hot springs are a function of geological, tectonic setting and their water chemistry is controlled by the host lithology.

The thermal features of the Hydrothermal System of Northwestern Algeria (HSNA) consist of thermal springs, sulfate precipitation zones, alteration zones and travertine deposits along open fractures giving rise to a horseshoe feature 800 m long and 10 m in thickness in the Bouhdjar geothermal zone. The temperature of discharged thermal waters ranges between 42.9 °C and 67.1 °C, with an artesian flow rate of 6 to 9 Ls^{-1}. Since Roman time to present, thermal waters of HSNA are mainly used for bathing to heal pulmonary problems, arthritis and rheumatism.

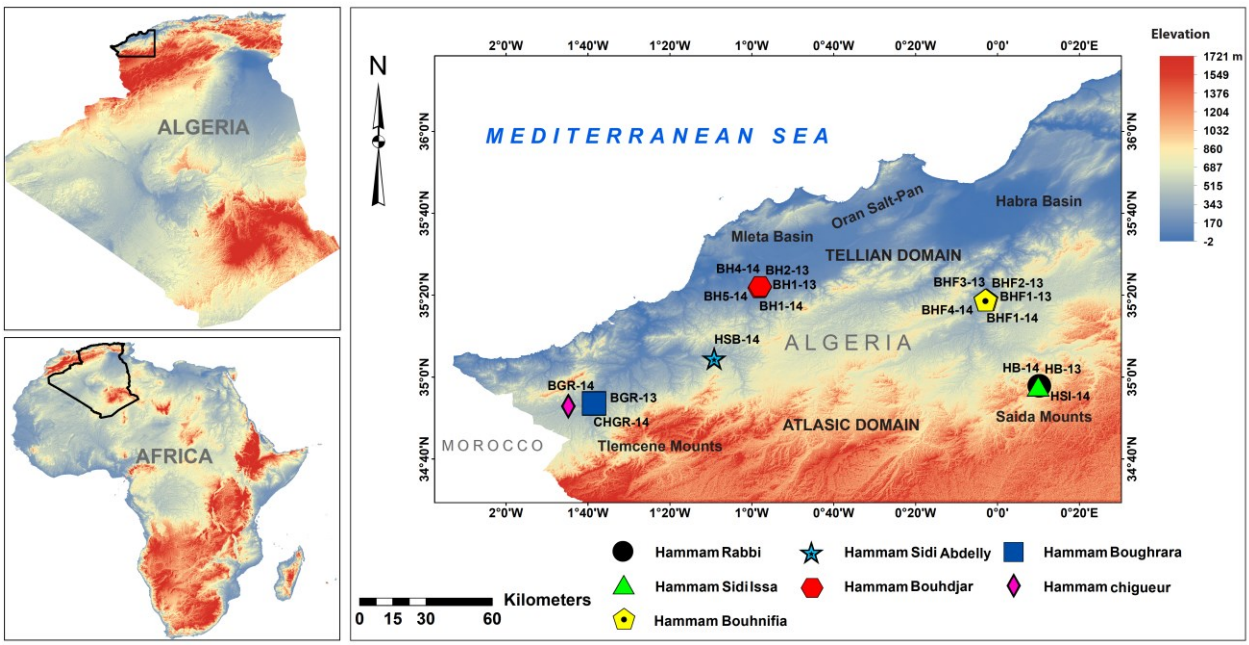

Figure 1: Location of hot springs sampling points in the study area in Northwestern Algeria.

After decades of evaluation of these geothermal features, little is known on the origin of the hydrothermal system of NW Algeria. Specifically, the controversy of the impact of closely volcanic activity in these geothermal features because of the distance and age of these volcanic bodies and a presence of possible plutons beneath spring vents (Issaadi, 1992). In order to give more evidence on the origin of the geothermal features, the objectives of this work are: (a) to evaluate the influence of geothermal gradients on meteoric waters (b) to investigate the origin of thermal waters to ascertain the link between Plio-Quaternary volcanism and these geothermal waters using stable isotopic data gas mixing models; and (c) to propose a geothermal conceptual model for HSNA based upon the geochemical characteristics of fluids discharged.

Different correlations are shown of the interaction of hot waters with the host lithology due to dissolution or precipitation of minerals which control the hot water chemistry. ii) estimating the maximum reservoir temperature using chemical geo-thermometers. iii) resolving the origin of the thermal waters.

2. GEOLOGY

The northern Algeria belongs to the North African margin and forms part of the Alpine Maghrebide belt that extends from Gibraltar to Sicily-Calabria (Auboin and Durand-Delga, 1971; Bouaziz et al., 2002; Domzig et al., 2006; Fourré et al., 2011). The Maghrebides are subdivided into two main structural domains: the Tellian Atlas "Tellian" in the north and the Saharan Atlas 'Atlasic foreland' to the south.

The HSNA (Hydrothermal System of Northwestern Algeria) area lies in the external zones of the Tellian Atlas namely Tellian zones by Wildi (1983), which are characterized by Miocene folds and nappes thrust over the Atlasic foreland (Saharan Atlas) where other zones of HSNA appears also (eg, HB,BGR, CHGR and HSI). The Tellian domain starts in the coastal Paleozoic shale massifs. These consist of a granitic and metamorphic basement overlain by Mesozoic clay and an evaporitic sequence. They are identified as a para-autochthonous Tellian substratum of Paleozoic to Jurassic age. They can be defined as a significant potential reservoir of HSNA. In the south, the Habra, Mleta and Tafna basins of Miocene and Plio-Pleistocene age are characterized by sandstones, clay and conglomerate developed during the early Miocene extensive phase. This extensional tectonic activity in the Mleta basin led to a flat area of salt pan (*Sebkha of Oran*). This is composed of a Messinian evaporitic sequence formed during the upper Miocene with the closure of Mediterranean Sea (Aifa et al., 2003). These basins form a groove that extends in a WSW-ESE direction and separates Paleozoic formation or para-autochthonous basement from the thrust sheets domain in the south (Fenet, 1975; Thomas, 1985). They are crossed by volcanic bodies (dykes or sills eg, in BGR geothermal zone in the Tafna basin. Their emplacement is spread over a period ranging from Miocene to Quaternary (Maury et al., 2000; Savelli, 2002). To the south, Tellian thrust sheet "nappes" or the allochtonous unit of Sebaa Shioukh is mainly made up of marl-sandstone with limestone intercalations of small thickness (5-10m) and forms a small aquifer (Perrodon, 1957; Fenet, 1975; Megartsi, 1985; Issaadi, 1996). This nappe domain is of Vraconian to Oligocene age and are divided in two sub-units: the first of Vracono-Senonian age and the second of Senono-Oligocene age (Issaadi, 1996). These thrust sheets after dislocated by gravity in early Miocene and have been displaced to the south during the late Miocene compressive deformation stage as Mediterranean Sea closed. The resultant shortening between the Iberian and Eurasian plates was approximately 3 to 6 mm/ year (Belabbes et al., 2008; Nocquet and Calais, 2004; Serpelloni et al., 2007).

In the south, the Atlasic domain appears as the Saida and Telemcene mountains. It is a morphostructural zone resulting from the superposition of several tectonic phase during the late Cretaceous. Most of the zones trend ENE-WSW to E-W (eg. Pays des Horsts in Tlemcene Mountain) and NE-SW (Middle Atlas and valley of Mouloya in Morocco). The Atlasic domain is overlain by Paleozoic to Jurassic formations, essentially shale, carbonate and dolomitic sequences which are often intruded by volcanic eruption and plutonic intrusion seen in the East to HB and HSI geothermal zones in Saida mountains.

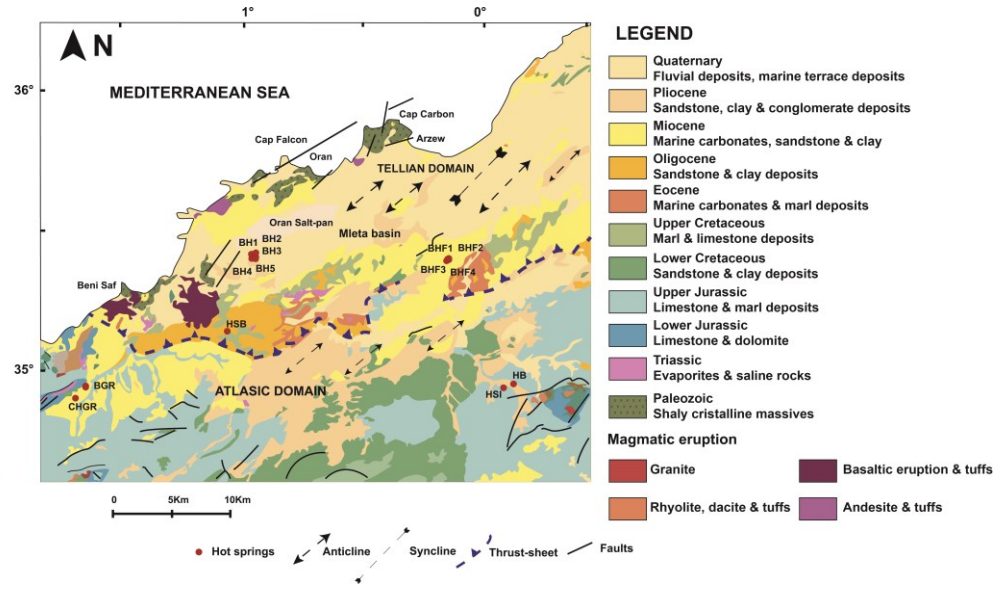

Figure 2: A Geological map showing the different lithology and structure of Northwestern Algeria (modified from Fenet, 1975).

Table1: Chemical (in mg/L), stable isotopes (in ‰) and dry gas (in %) composition of the thermal waters collected from HSNA.

ID SAMPLE	T (°C)	pH	Cond (µS/cm)	TDS (mg/L)	Na (mg/L)	K (mg/)	Li (mg/L)	Ca (mg/L)	Mg (mg/L)	Cl (mg/L)	SO_4 (mg/L)	HCO_3 (mg/L)	F (mg/L)	Br (mg/L)	B (mg/L)	As (mg/L)	SiO_2 (mg/L)	δD (‰)	$\delta^{18}O$ (‰)	O_2 vol.%	N_2 vol.%	Ar vol.%	He vol.%
BGR-14	44.8	6.94	739		175	19.7	0.015	53.6	30.7	63.4		296	0.17		0.07	0.008		–	–				
BGR-13	42.9	7.53	730	492	103	7		28	13	69	21	296					26.0	-48	-7.2				
CHGR-14	31.8	6.82	5020	3163	861	9.97	0.17	147	47.0	1410	200.2	317.3	0.35	1.018	0.13	0.006	26.30	–	–				
BH1-14	65.4	6.11	5650	3677	796	48.3	1.37	312	37.4	1490	56.90	778.0	1.97	1.274	1.35	0.023	57.08			20.17	78.83	0.9899	4.857
BH1-13	66	6.45	5720	3693	950	46		310	35	1650	60	656					65.7	-48	-7.6				
BH2-14	50.7	6.21	5620	3743	825	49.2	1.42	281	38.1	1580	58.89	591.8	2.24	1.283	1.68	0.025	61.41			19.00	80.04	0.9512	3.607
BH2-13	66.1	6.2	2460	1523	1010	60		351	46	1890	30	622					63.7	-47	-7.2				
BH3-14	42.5	6.25	5150	3575	788	48.9	1.36	335	36.5	1520	57.102	839.0	2.09	1.2409	1.51	0.013	57.08						
BH4-14	43.2	6.15	5630	3794	798	46.1	1.36	338	36.7	1520	56.91	829.8	2.10	1.269	1.54	0.010	58.36	–	–				
BH5-14	41	6.33	5700	3638	888	60.4	1.38	339	37.0	1520	55.84	823.7	1.74	1.234	1.55	0.016	56.32						
BHF1-14	66.3	5.94	2380	1351	262	25.1	0.50	168	36.7	373	93.73	701.7	1.86	0.5194	0.56	0.010	44.11	–	–	20.76	78.29	0.9408	2.031
BHF1-13	64.5	6.38	2380	1553	264	25		177	28	409	80	610					46.4	-47	-7.1				
BHF2-14	62.6	6.28	2400	1320	276	30.3	0.47	158	36.4	378	93.11	671.2	1.95	0.5182	0.55	0.009	42.58	–	–				
BHF2-13	66.1	6.2	2460	1523	255	25		201	24	397	97	586					45.4						
BHF3-14	44.3	6.21	2510	1416	302	27.9	0.45	166	44.4	386	152.2	613.2	1.96	0.6757	0.53	0.012	39.02						
BHF3-13	52.8	6.59	2350	2142	318	27		153	31	391	98	650					45.9						
BHF4-14	52.5	6.35	2370	1328	259	32.0	0.48	163	37.0	366	102.3	637.6	1.76	0.5472	0.54	0.11	41.57	–	–				
HB-14	46.2	6.43	2520	1868	300	15.4	0.12	213	40.5	379	540.9	311.2	1.15	0.5238	0.19	0.019	43.09			18.78	80.24	0.96355	2.9556
HB-13	45.9	6.81	2670	1742	300	13		234	32	398	486	320					43.9	-56	-8.1				
HSI-14	45.5	6.87	3540	2792	412	17.2	0.18	318	58.7	555	913.3	317.3	1.49	0.6860	0.25	0.048	50.72						
HSB-14	34.4	6.82	768	443.0	28.0	2.23	<0.01	89.1	34.2	47.4	13.28	414.9	0.03	0.1339	0.03	0.0008	13.12						

In the northernmost part of the region, between the Ain Timouchent and Beni Saf areas, a post-collisional magmatic activity of calc-alkaline and alkali-basaltic type took place, which is mainly related to the regional tectonic process occurring along a NE-trending belt extending from the Alboran zone to the Tellian sector in Algeria and the middle Atlas and the Anti-Atlas in Morocco. This activity has a geochemical signature similar to an intra-oceanic island basalt (Chalouan, 2008).

For this Neogene orogenic magma of northwestern Algeria, the age of the calc-alkaline type ranges between 7.5 and 11.5 Ma, while the age of the alkali-basaltic type ranges only from 0.8 to 3.9 Ma (Coulon et al., 2000; Louni-Hacini et al., 1995).

3. WATER CHEMISTRY

3.1 Chemistry of Major Ions

Collected water samples from the two different zones of HSNA; a) Tellian sector and b) Atlasic foreland, highlight a significant heterogeneity in their chemical-physical features. The outlet temperature ranges (T from 31.8 °C to 66.3°C) reported in Table 1. The thermal waters of HSNA displays a near neutral pH values ranging from 6.1 to 7.5, noting an efficient positive relationship between salinity, pH value and chloride amount in HSNA zone (a) most notably in BH geothermal zone. TDS value is up to 3794 mg L^{-1} and probably reflects longer circulation and residence times.

According to the Piper and Ternary diagram (Fig. 2a and b), thermal waters from distinct zones of HSNA and on the basis of TDS, EC and pH can be classified in details into five groups

(i) Group 1 Na-(Ca)-Cl-(HCO_3): hot waters from low altitude 154 m –159 m mainly from BH geothermal zone including thermal springs BH1-13, BH1-14, BH2-13, BH2-14, BH3-14, BH4-13, BH5-14, with an EC in the range of 2460-5560 µS/cm and pH from 6.1 to 6.87, chloride is the dominant anion, and the major cation is Na, Ca and HCO_3 are present but in secondary position.

(ii) Group 2 Na-(Ca)-HCO_3-(Cl): hot waters coming mainly from BHF geothermal zone of an altitude 212 m-254 m including thermal springs BHF1-13, BHF1-14, BHF2-13, BHF2-14, BHF3-14, BHF3-13, BHF4-14 with an EC in the range of 2350 -2510 µS/cm and pH from 5.94 to 6.59. Unlike to the first group bicarbonate, HCO3 is the dominant anion followed by Cl; the major cations are Na and Ca.

(iii) Group 3 Na-HCO_3: hot waters coming mainly from Tlemcene basin BGR and CHGR hots springs with an altitude of 264 m and 354 m respectively and an EC of 730 to 739 µS/cm and pH 6.94 to 7.53 of for BGR geothermal zone while with high mineralized water in CHGR of 5020 µS/cm and pH of 6.82. The dominant anion is bicarbonate HCO3 and the dominant cation is Na.

(iv) Group 4 Ca-HCO_3: hot water from HSB hot spring in south of Tellian zones (a) with an altitude of 355 m and low EC of 768 and pH of 6.82. The major anion is HCO_3 and the major cation is Ca.

(v) Group 5 Na-Ca-SO_4: hot waters of high altitude of Saida Mountains of HB geothermal zone and HSI geothermal zone, zone (b) of HSNA, with an altitude of 623m - 625m with an EC in the range of 2520-3540 µS/cm and pH from 6.43 to 6.87. The dominant anion is sulfate SO_4; the major cations are Na and Ca.

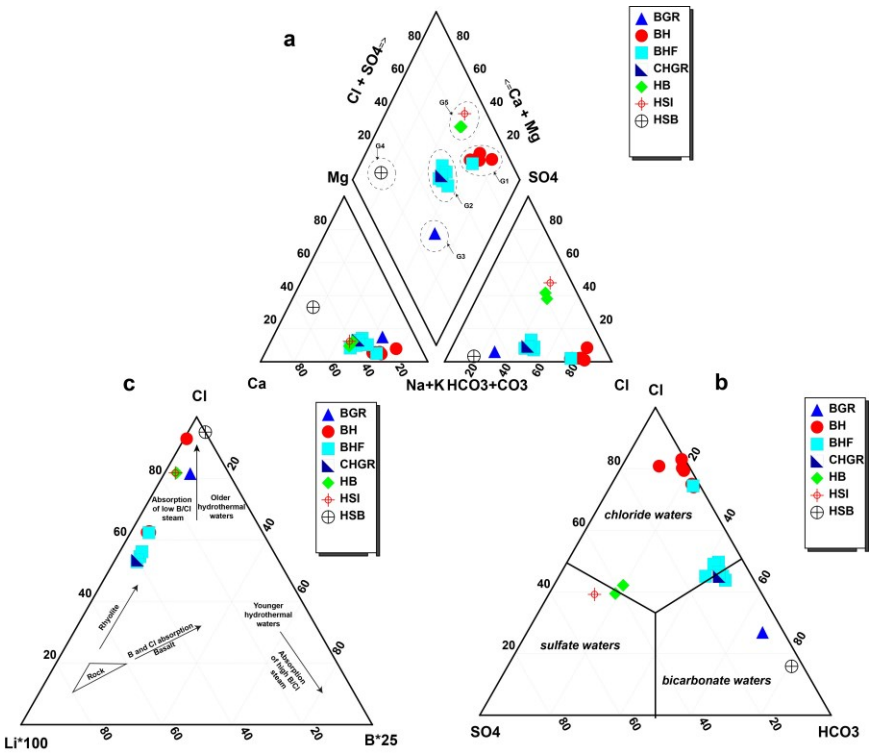

Figure 3: (a) Piper diagram showing HSNA hot spring samples (mg/L); (b) Ternary diagram of Cl-SO_4-HCO_3, showing the water types of the HSNA, (c) Cl-Li*100-B*25 ternary plot for HSNA samples.

3.2 Minor and Trace Elements

Generally, the concentration of minor and trace elements in thermal waters exceed those of cold groundwater. This is because the increased reactivity hot waters tend to act as a chemical sink for minor elements from the host rock through weathering (Ma et al., 2011). Arsenic (As) content in the majority of samples of HSNA generally exceeds 10 µg/L except (CHGR BGR, and BHF2) and represents the maximum permitted value for drinking. Arsenic is a usual component of geothermal fluids and volcanic gases. It can be either a major element in some sulfides, as arsenopyrite or secondary element in pyrite, its enrichment can be explained by an interaction between thermal waters and sulfide-rich rock most probably Triassic pyrite.

Chloride waters of BH exhibits a significant concentration of B (1350 µg/L to 1680 µg/L), Li (1370 µg/L to 1420 µg/L), Br (1234 µg/L to1283 µg/L) and Cs (130 µg/L to 150 µg/L). This is of less significance toward the south for bicarbonate-chloride BHF waters. Thus presence of the elements Br, Li, B may have two potential origin. Firstly, the Br/Cl ratio of circa 1.9×10^{-3} in chloride waters, reaching a maximum of 3.9×10^{-3} in the bicarbonate-chloride waters of BHF and exceeding a maximum possible from Sea water origin about 1.57×10^{-3} (Herczeg and Edmunds, 2000). Or secondly. Br/Cl ratio may due to halite dissolution ratio during flow through Triassic evaporites as they travel to the ground-surface. The interaction with Triassic or Messinan evaporites during flow to the ground-surface may also be another potential source of trace element although Br/Cl exceed 0.02×10^{-3} which is the ratio of halite dissolution (Herrmann, 1972).

4. CHEMICAL GEOTHERMOMETERS

Solute geothermometers, which are mainly based on temperature-dependent mineral fluid equilibria, are considered as valuable tools to assess the geothermal reservoir temperatures. The following geothermometers were applied to estimate HSNA reservoir temperatures as shown in Table 2: (A): Na-K-Ca (Fournier and Truesdell, 1973) using β=1/3; (B) Na/K (Nieva and Nieva, 1987); (C): Na/K (Fournier, 1979); (D): Na/K (Truesdell, 1976); (E): K/Na (Giggenbach, 1988); (F): K/Mg (Giggenbach, 1988); (G): silica (Giggenbach, 1992).

The fast equilibrating K/Mg (Giggenbach, 1988) geothermometers seems to be more influenced by dissolution of host rock rather than by water/mineral equilibrium, (as K in BGR-13 ~19 and gives 97°C), meanwhile it gives a satisfied results in SO_4 waters of HB and HSI (HB~108 and 109°C ; HSI~110°C) whilst (G): silica (Giggenbach, 1992) gives temperature quite close and slightly higher to discharge temperature and should only be taken as minimum temperatures for waters of HSNA and can mainly imperatively due to cooling and mixing of rich silica hot waters with colder and deficient shallow groundwater. (A): Na-K-Ca (Fournier and Truesdell, 1973) geothermometers infers too high temperatures estimations especially in carbonated rich in Ca waters (BHF4-14 ~212°C) and seems to be more affected by calcite dissolution in contrast with (D): Na/K (Truesdell, 1976) that gives too low temperatures and even less than discharge temperature (BH1-14~59°C), it is important to apply Na/K geothermometers cautiously because of dissolution of halite leaching Na ions into waters from Messinian and Triassic host rocks. The most reliable and reasonable temperatures for HSNA is (C): Na/K (Fournier, 1979) giving (BH1-14~112°C), whereas (B) Na/K (Nieva and Nieva, 1987) and (E): K/Na (Giggenbach, 1988) can be taken as maximum reservoir temperature.

To ascertain the appropriate SiO_2 phase implicated in the equilibration of HSNA thermal waters, log (C^2K/CMg) versus the log ($CSiO_2$) diagram is established within three solubility curves for amorphous silica, chalcedony and quartz, respectively (Henley and Ellis, 1983). In fact, most of samples of HSNA are plotted between the chalcedony and quartz dissolution curves and infers temperature lesser than 100°C as the solubility is only controlled by chalcedony while chalcedony geothermometers usually infers discharge temperature. Since the fractured reservoir rocks mainly composed by limestones and dolomite are the rule, it is likely that application of the quartz gothermometers is restricted. The samples from Atlasic domain including HSB are plotted above chalcedony curve, and following the log (C^2K/CMg) vs the log ($CSiO_2$) diagram (Fig. 4a) the mixing trend in BH zone goes downward from BH2-13 to BH1-14 with increased Mg content in waters.

The ternary diagram of $Na/1000\text{-}K/100\text{-}Mg^{1/2}$ (Fig. 4b) suggested by Giggenbach (1988) is mainly used to infer reservoir temperatures and though helps identify the fluid maturity of waters that reaches the equilibrium with the host rock to determine their applicability for geothermometry and ascertain the mixing effect. All thermal waters from HSNA are plotted in the immature water field rather close to $Mg^{1/2}$ corner. This effect can be explained by the mixing of the hot equilibrated waters with cooler Mg-rich groundwater feed from the dissolution of the Jurassic dolomitic sequence that leaches Mg into the water and which makes the reliability of cation geothermometers week and cautious.

The combined K^2/Mg vs K^2/Ca geothermometers of (Fournier and Truesdell, 1973) is among valuable graphic approaches to determine degree of water-rock equilibrium, reservoir temperatures and PCO_2 of geothermal liquids (Fig. 4c) most of samples of HSNA fall out of the temperature range of the geothermal interest and show immature condition, giving temperature between 80 to 100 °C for BHF and BH water samples. The samples are plotted between “calcite formation” line and equilibrium line and holding a high PCO_2 values and which favors the conversion of Ca-Al silicate to calcite of the water samples. This high log PCO_2= 0.01bar especially in BH thermal waters bearing higher amounts of dissolved CO_2 up to 58.4 mg/L could be probably linked to an additional mantle degassing for this thermal water.

Table 2: Estimated reservoir temperatures (°C) of HSNA water samples using several cationic and silica geothermometers.

ID SAMPLE	T Na/K T	T Na/K F	T Na/K N	T K/Na G	T K/Mg G	Na-K-Ca (beta 0.333)	T SiO_2 G
BGR-14	57	111	95	126	97	209	
BGR-13		45	33	63	114	177	46
CHGR-14					123	115	46
BH1-14	59	112	96	127	77	186	85
BH1-13	50	104	88	119	77	177	93
BH2-14	59	112	96	127	76	186	89
BH2-13	63	116	100	131	74	188	91
BH3-14	60	113	97	128	76	186	85
BH4-14	56	109	93	125	77	182	86
BH5-14	68	120	104	135	71	193	84
BHF1-14	58	111	95	127	93	196	71
BHF1-13	57	111	95	126	89	195	74
BHF2-14	69	121	105	136	88	206	69
BHF2-13	59	112	96	127	87	195	73
BHF3-14	60	113	97	128	93	197	65
BHF3-13	55	109	93	124	89	194	73
BHF4-14	75	127	110	141	87	212	68
HB-14		72	58	89	108	163	70
HB-13		59	46	77	109	154	71
HSI-14		69	55	86	110	155	79
HSB-14					169	153	18
SH-14		76	61	92	88	163	74

T Na/K T; (D): Na/K

(Truesdell, 1976)
T Na/K F; (C): Na/K (Fournier, 1979)
T Na/K N; (B) Na/K (Nieva and Nieva, 1987)
T K/Na G; (E): K/Na (Giggenbach, 1988)
T K/Mg G; (F): K/Mg (Giggenbach, 1988)
Na-K-Ca (beta 0.333); (A): Na-K-Ca (Fournier and Truesdell, 1973) using $\beta=1/3$
T SiO_2 G; (G): silica (Giggenbach, 1992)

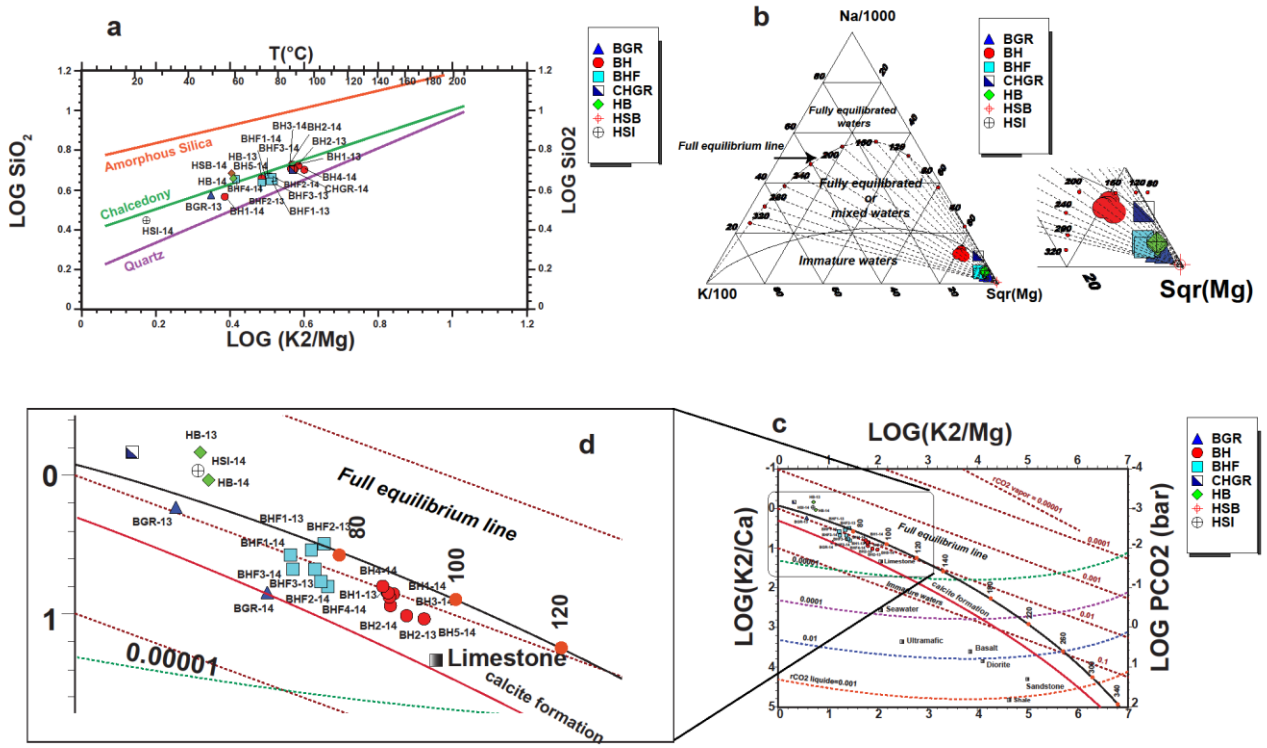

Figure 4: (a) log (C^2K/CMg) vs the log ($CSiO_2$) diagram, (b) Ternary Na-K-Mg diagram (mg/L) for HSNA water samples (Giggenbach, 1988), (c) log K^2/Mg vs log K^2/Ca diagram for HSNA water samples.

5. GAS CHEMISTRY

The relative abundances of the major gas species (N2, O2, CO2, Ar, He) in the dry gas phase at equilibrium with each water sample from HSNA are presented in two ternary plot shown in Fig 5. And indicate that all samples exhibits N2 dominated composition (from 72.28 to 77.18 vol. %) whilst oxygen represents a relatively moderate proportion (from 17.74 to 19.47 vol. %) with a small fraction of Argon (from 0.86 to 0.95 vol. %) supporting a likely atmospheric derivation of the dissolved gasses. According to N2–Ar×100–He×1000 triangular diagram Fig. 5a, N2/Ar (from 79.63 to 84.15) and all samples of HSNA are plotted rather close to Air saturated water field whose N2/Ar ratio is ~84. However, He/Ar (from 2.2×10-2 to 4.9×10-2) and N2/He (1,623 to 3,855), respectively, can be explained by the high residence time and so, the increased Helium can be also leached from young alkali-basaltic rock of 0.7MA rather than 'He' outgassed from a magmatic input. The atmospheric contribution in terms of N2/O2 (from 3.77 to 4.22) is approximating ASW value ~ 2 and values are similar to (eg. Winton and Weston hot springs of the Galilee basin in Australia) and considered as air-enriched. Therefore, the dissolved O2 appears to be mainly due to local infiltration of shallow waters and/ or contamination of the deep artesian groundwaters by shallow air equilibrated waters. In the O2–He×100–CO2 mixing model Fig. 5b, the moderate CO2-enrichement (from 3.43 to 7.66 vol. %) observed in thermal springs from Tellian zones (BH2 and BHF1) suggests the involvement of an additional CO2 source in hot waters than only atmosphere.

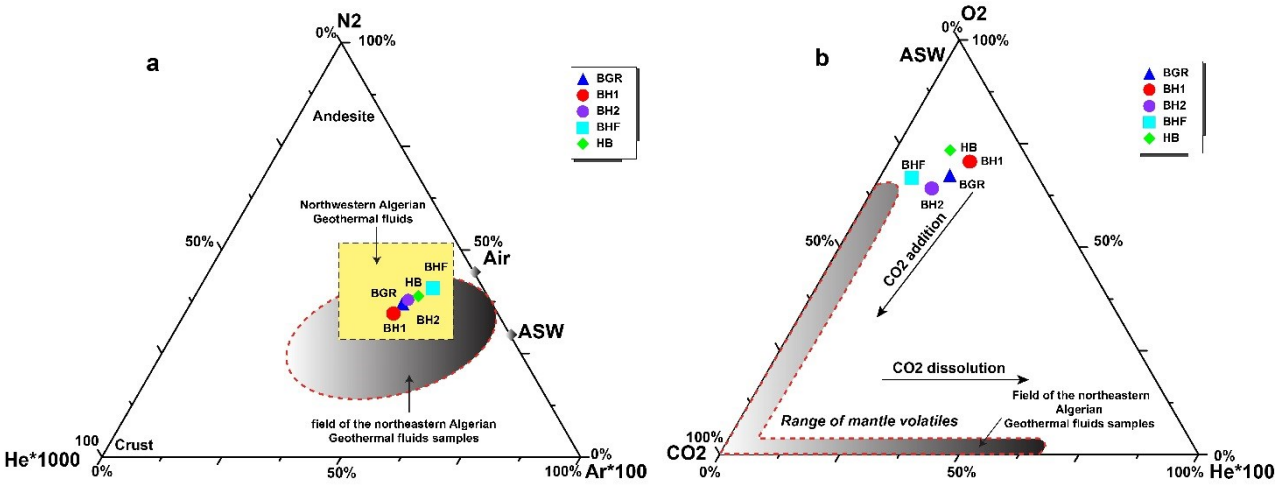

Figure 5: (a) N_2-Ar*100-He*1000 Ternary mixing model, (b) O_2-CO_2-He*100 gas mixing model for HSNA thermal waters, ASW denotes Air Saturated Water.

6. STABLE ISOTOPES

The isotopic signature of thermal waters can act as a tracer of the fluid origins and reservoir processes in geothermal systems (Craig et al., 1956; Craig, 1963; White, 1986). The isotopic data of δ^{18} O and δ D are quite variable ranging from -8.1 to -7.1‰ and from -56 to -47‰, respectively (Fig. 6).

Collected samples from HSNA fall along the Global World Meteoric Line (GMWL; Fig. 6), the equation for which is δ D = 8.13 δ^{18} O+10.8 (Rozanski et al., 1993), indicating a meteoric origin for the thermal waters. The absence of an oxygen shift toward a positive value indicates that there is no isotopic exchange with the host rock and that the thermal waters belong to a low-enthalpy resource. Thus, waters infiltrated through a deep-seated fault network and became heated during deep advective flow. The recharge probably takes place at fractured Jurassic limestone. However, depletion of δ^{18} O toward a less negative value at BH1 compared to BH2 is likely due to mixing with shallower cold groundwater with lower Cl^- content, mainly by carbonated aquifers of Miocene age of H. Bouhdjar. The downwards shifting of δ D of the collected samples relative to local meteoric water reflects the high altitude of the spring discharge and distance from seawater further to the south (altitude and latitude), i.e., HB ~ 637 m. ASL, δ D = -56 ‰.The light isotopic value of δ D in Group 1 with the higher Cl^- content water (BH1 and BH2) is due to a long residence time and a deeper circulation indicating that these groundwaters belong to a fossil reservoir.

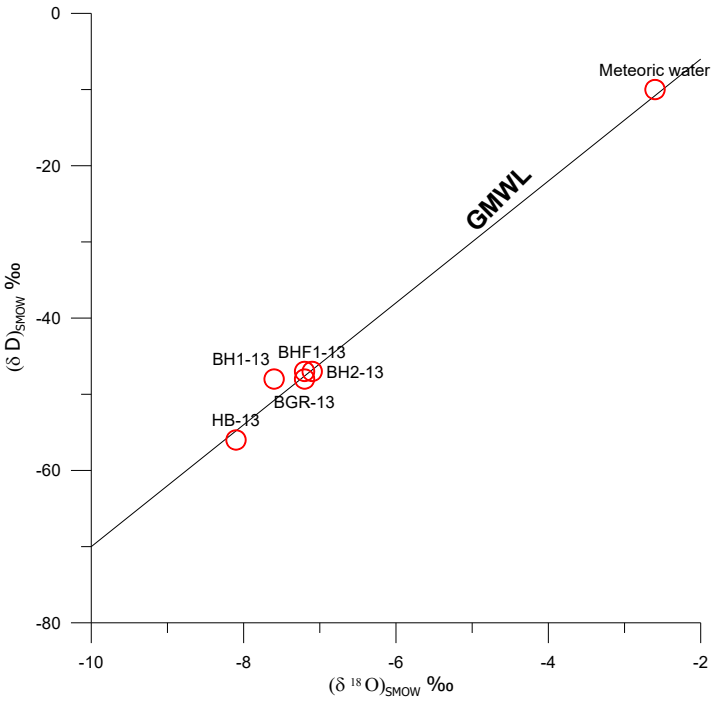

Figure 6: Isotopic composition of thermal waters and local meteoric water from northwestern Algeria; all compositions lie close to global meteoric world meteoric line (GMWL)

5. DISSCUSSION

5.1 Mixing models

5.1.1 Silica mixing model

An enthalpy-silica mixing model suggested by Fournier and Truesdell (1974) and Truesdell and Fournier (1977) was applied to infer the temperature of the hot water component in mixed water and to estimate reservoir temperatures of northwestern Algerian thermal waters. Enthalpy values used to estimate northwestern Algerian reservoir temperatures were derived from measured spring discharge temperatures and the steam table (Keenan et al., 1969), and meteoric water was used as the reference cold water. Relating the cold sample water to thermal waters, within separation and steam escape (100 °C, 419 KJ/kg), yields points a, b, c, d, and e in Fig. 7b. Thus, the reservoir temperature 478 KJ/Kg, 532 KJ/Kg, 560 KJ/Kg, 651 KJ/Kg, is determined by connecting horizontal lines to the quartz solubility curve corresponding to the maximum steam line in BH1, BH2, HB, and BHF3, while a vertical line from a', b' and c' intersected with the quartz solubility no steam loss curve at indicating the original silica concentration in the reservoir The fraction of the hot water component in the spring discharge lost as steam before mixing (Xs) is given by Xs = 1 - ($SiO_{2at\ (PSa', PSb', PSc')}$/$SiO_{2at\ (a', b', c')}$), and it ranged between 0.14 and 0.15. The intersection of cold meteoric water with the no steam loss curve yields estimated temperatures d' BHF1 and BHF2 and e' BGR, which indicates the composition of the parent geothermal water prior to mixing. Results obtained by the silica-enthalpy model were slightly higher than those estimated by different silica geothermometers and ranged between 108°C to 161°C and an original silica in reservoir of 160 mg/L as maximum. These results denote that this over-estimated temperature is likely due to silica precipitation caused by mixing with cold water and cooling.

5.1.2 Chloride mixing model

The enthalpy-chloride mixing model of Fournier (1979) is a powerful tool for characterizing the parent geothermal liquid for HSNA thermal waters and delineating their upflow and cooling process in order to determine the hydrologic complexities of the different hydrothermal systems and to estimate the reservoir temperatures (Multu, 1998; Guo et al., 2009; Guo and Wang, 2012). Two principal trends can be inferred from Fig.7a: (1) conductive cooling, where the fluid loses heat to the surrounding host rock and enthalpy increases but the chloride content remains constant. This process is detected in both low and high Cl^- springs (BHF1, BHF2, BHF3, HB and BH2. (2) Mixing with cold groundwater that is less enriched in Cl^-, which produces a decrease in the enthalpy and Cl^- content. This process occurred clearly at BH1, which is mixed with BHC (cold groundwater near Hammam Bouhdjar).

The high Cl^- content in thermal water supplied by a salt pan (Sebkha of Oran) through dissolution of Na and Cl^- from halite minerals and the presence of NE-SW trending fault zone structures that increase the mixing ratio. The estimated temperatures of the parent geothermal liquid in BH geothermal zone are approximately 131°C, which approximates those estimated by (C): Na/K (Fournier, 1979) in the two hot springs. However, the parent geothermal liquid of BHF1, BHF2 and BHF3 of Hammam Bouhnifia yields temperatures of approximately 132°C, which is also close to Na/K (Giggenbach, 1988) because Na/K ratio is less affected by NaCl dissolution rather than Ca increase within calcite dissolution in carbonated water of BHF geothermal field.

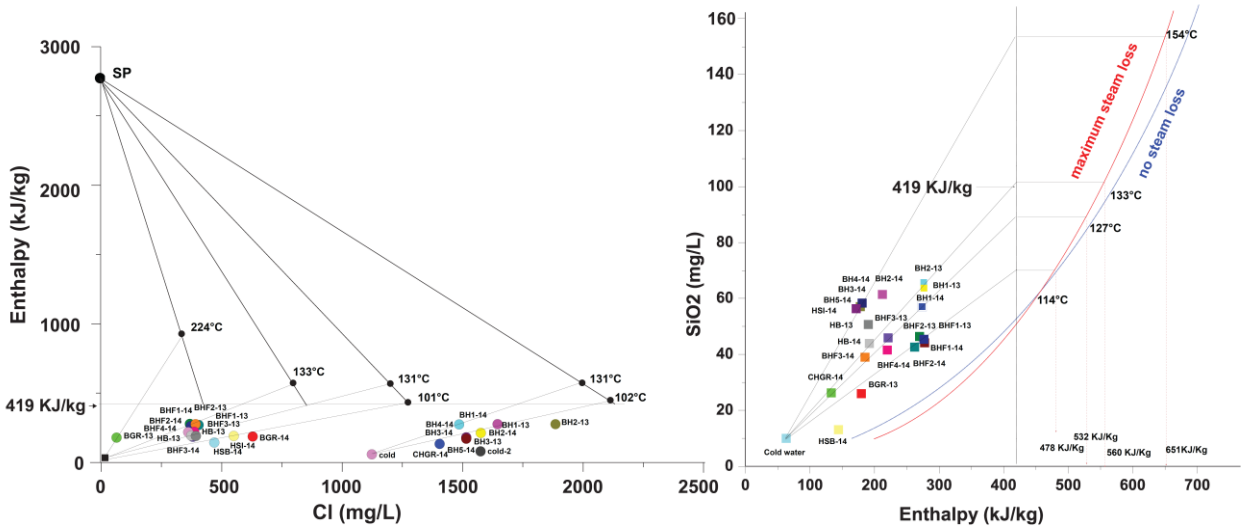

Figure 7: (a) Chloride-Enthalpy mixing model, showing mixing trends for hots springs water of HSNA, (b) Silica enthalpy mixing model showing estimated reservoir temperatures for HSNA waters.

5.2 Geochemical Conceptual Model

According to stable isotope data ($\delta^{18}O$ and δD) and gas mixing models, the meteoric water recharged from higher altitude (Tlemecen Mountain at 1100 mASL; Saida Mount 1350 mASL) circulated through deeper fault networks acting as a conduit for uprising water and saline sediment. The high heat flow of northwestern Algeria is due to the tectonic setting (80-140 mW/m^2; Rimi et al., 2012) and supplies the required heat to the geothermal system with an advective heat output (capacity) of ~ 0.55 MWt (HB); ~ 1.24 MWt (BHF1, BHF2, BHF3); and ~0.5 MWt (BGR) (Saibi, 2015).

Ascending thermal water is conductively cooled and loses heat to surrounding host rock or is mixed with cooler Mg-rich shallow groundwater that is mainly responsible for the temperature decrease (e.g., in Hamman Bouhdjar with a mixing ratio R=31%). Assuming a higher geothermal gradient in the northwestern part of Algeria, which can reach 42.8°C km^{-1} (Bouchareb-Haouchine, 2012), $T = T_0 + \frac{\partial T}{\partial Z} Z$, where T_0 is a surface temperature of approximately 15°C and $\frac{\partial T}{\partial Z}$ represents the geothermal gradient of northwestern Algeria. Therefore, the circulation depth Z is about 2.1 to 2.6 km at BH geothermal zone; 2.4 km for HB and HIS, and 3 km for BHF1, BHF2, and BHF3. This depth according to the geological cross-section corresponds to the fractured and dense Jurassic dolomite and limestone sequence acting as a reservoir.

5. CONCLUSION

Thermal waters from northwestern Algeria (HSNA) show complex features linked to the heterogeneous lithology and the complex geodynamic context, therefore, the following concluding remarks summaries this study and gives answers to the several questions at the top of this manuscript;

1) Thermal waters from HSNA are classified as five types (Na-(Ca)-Cl-(HCO_3): Na-(Ca)-HCO_3-(Cl); Na-HCO_3; Ca-HCO_3; Na-Ca-SO_4.
2) The chemistry of thermal water is strongly influenced by the lithology, the fractured dolomitic sequence of Jurassic age as reservoir in whole area, whilst Na-Cl, and Ca-SO_4 features come directly from the Triassic and Messinian evaporitic sequence halite/gypsum bearing rocks, increasing dissolution and leaching Na, Ca, SO_4 into waters.

3) Trace elements determine to potential origin according to the amount of chemical species in waters, first, from Sea water or interacted with marine sediment, second and the less probable is from dissolution of halite mineral of evaporitic rocks.
4) Gas ternary mixing models, stable isotopes ascertain the meteoric origin for thermal waters, and Air saturated water type revealing a possible mixing with cold ground water. The contribution of volcanic inputs beneath hot springs in northwestern Algeria in heating, despite the higher heat flow 80-140 $mW/m^{2,}$ should be rejected as they are non-volcano-genetic. The major involvement of intrusive and eruptive bodies in NW Algeria, in leaching with chemical as Na, K, Mg thermal water by weathering and alteration.
5) The most reliable temperatures are estimated Na/K Fournier, silica mixing model gives also temperatures closer to Na/K Fournier, while the highest temperatures are recorded by Na-K-Ca, because of dissolution of Ca from carbonate and dolomite. Silica gothermometers infer temperatures lower than discharge temperature and makes its result not reliable.

REFERENCES

Aïfa. T., Feinberg, H., Derder, M.E., and Merabet, N.E.: Contraintes magnétostratigraphiques concernant la durée de l'interruption des communications marines en Méditerranée occidentale pendant le Messinien supérieur, *Geodiversitas*, **25**, (2003), 617-631.

Auboin. J., and Durand-Delga, M.: Aire mediterraneenne, *Encyclopidia universalis,* **10**, (1971), 743–745.

Belabbes, S., Meghraoui, M., Cakir, Z., and Bouhadad, Y.: InSAR analysis of a blind thrust rupture and related active folding: the 1999 Ain Temouchent earthquake (Mw5.7, Algeria) case study, *J Seismol*, **13**, (2008), 421-432.

Bouaziz, S., Barrier, E., Soussi, M., Turki, M., and Zouari, H.: Tectonic evolution of the northern african margin in Tunisia from paleo stress data and sedimentary record, *Tectonophysics*, **357**, (2002), 227–253.

Bouchareb-Haouchine, F.Z : Etude Hydrochimique des Sources Thermales de l'Algérie du Nord- Potentialités Géothermiques. *Thèse Doctorat Es Science, USTHB*, Algiers, (2012), p. 135.

Chalouan, A., Michard, A., El Kadiri, K., Negro, F., Frizon de Lamotte, D., and Saddiqi, O.: The Rif belt, In: Michard, A., Chalouan, A., Saddiqi, O., Frizon de Lamotte, D (eds). Continental evolution: the geology of Morocco. Springer, Berlin, (2008), 203–302.

Coulon, C., Megartsi, M., Fourcade, S., Maury, R.C., Bellon, H., and Louni-Hacini, A.: The transition from the calc-alkaline volcanism during the Neogene in Oranie (Algeria): magmatic expression of a slab breakoff. *Lithos*, **62**, (2000), 87-110.

Craig, H.: The isotopic geochemistry of water and carbon in geothermal area. In: Tongiori, E. (ed), Nuclear geology in geothermal areas, Spoleto. Consiglio Nazional delle Riecerche, Laboratorio di Geologia Nucleare, Pias, (1963), 17-53.

Craig, H., Boato, G., White, D.E.: Isotopic geochemistry of thermal waters. *National Acad. Sci. National Research Council Publication*, **400**, (1956), 29-38.

Domzig, A., Yelles, A-K., Le Roy, C., Déverchère, J., Bouillin, J-P., Bracene, R., Mercier de Lépinay, B., Le Roy, P., Calais, E., Kherroubi, A., Gaullier, V., Savoye, B., and Pauc, H.: Searching for the Africa–Eurasia Miocene boundary offshore western Algeria (MARADJA'03 cruise), *C R Geosci*, **338**, (2006), 80–91.

Fenet, B.: Recherche sur l'Alpinisation de la Bordure Septentrionale du Bouclier Africain à Partir de l'Etude d'un Elément de l'Orogenèse Nord Maghrébine, Les Monts du Djebel Tessala et les Massifs du Littoral Oranais, *Thèse de Doctorat d'Etat*, (1975).

Fournier, R.O.: A revised equation for Na/K geothermometer, *Geoth Res Council Trans*, **3**, (1979), 221-224.

Fournier, R.O., and Truesdell, A.H.: An empirical Na–K–Ca geothermometer for natural waters, *Geochimica et Cosmochimica Acta,* **37**, (1973), 1255-1275.

Fournier, R.O., and Truesdell, A.H.: Geochemical indicator of subsurface temperature—part 2, estimation of temperature and fraction of hot water mixed with cold water. *J Res US Geol Survey*, **2**, (1974), 263-270.

Giggenbach, W.F.: Geothermal solute equilibria. Derivation of Na-K-mg-Ca geoindicators, *Geochim Cosmochim Acta*, **52**, (1988), 2749–2765.

Fourré, E., Di Napoli, R., Aiuppa, A., Parello, F., Gaubi, E., Jean-Baptiste, P., Allard, P., Calabrese, S., and Ben Mamou, A.: Regional variations in the chemical and helium–carbon isotope composition of geothermal fluids across Tunisia, *Chem Geol*, **288**, (2011), 67–85.

Giggenbach, W.F.: Isotopic composition of geothermal water and steam discharges. In: D'Amore, F., (Coordinator) Application of geochemistry in geothermal reservoir development, *UNITAR/UNDP, Vial del Corso*, Italy, (1992), pp. 253–273.

Guo, Q., Wang, Y.: Geochemistry of hot springs in the Tengchong hydrothermal areas, Southwestern China, *J Volcanol Geotherm Res*, **61-73**, (2012), 215-216.

Guo, Q., Wang, Y., and Liu, W.: Hydrogeochemistry and environmental impact of geothermal waters from Yangyi of Tibet, China. *J Volcanol Geotherm Res*, **180**, (2009), 9-20.

Herczeg, A.L., Edmunds, W.M.: Inorganic ions as tracers. In: Cook, P.G., Herczeg, A.L. (Eds.), Environmental Tracers in Subsurface Hydrology. Springer US, Boston, MA, (2000).

Herrmann, A.G.: Bromine distribution coefficients for halite precipitated from modern sea water under natural conditions. *Contrib. Mineral. Petrol*. **37**, (1972), 249–252.

Issaadi, A.: Le Thermalisme dans son Cadre Geostructural, Apport à la connaissance de la structure profonde de l'Algérie et de ses Ressources Géothermales, *Thèse Doctorat d'Etat, Univ.Sci.et Tech*, Alger, (1992).

Issaadi, A. Mécanismes de fonctionnement des systèmes hydrothermaux Application aux eaux thermo-minérales algériennes et aux eaux de Hammam Bou-Hadjar. *Bulletin du Service Géologique de l'Algérie*, **7(1)**, (1996), 71–85.

Keenan, J.H., Keyes, F.G., Hill, P.G, and Moore, J.G.: Steam tables, Wiley, New York, (1969), 162.

Louni-Hacini, A., Bellon, H., Maury, R.C.: Datation 40K-40Ar de la transition du volcanisme calco-alcalin au volcanisme alcalin en Oranie au Miocène supérieur, *Comptes Rendus Académie des Sciences*, Paris **321**, (1995), 975-982.

Ma, R., Wang, Y., Sun, Z., Zheng, C., Ma, T., and Prommer, H.: Geochemical evolution of groundwater in carbonate aquifers in Taiyuan northern China. *Appl. Geochem*, **26**, (2011), 884–897.

Maury, R. C., Fourcade, S., Coulon, C., El Azzouzi, M., Bellon, H., Coutelle, A.: Post-collision neogene magmatism of the Mediterranean Maghreb margin: a consequence of slab Breakoff. *Comptes Rendus de l'Académie des Sciences Paris*, **331**, (2000), 159–173.

Megartsi, M.: Le volcanisme mio-plio-quaternaire de l'Oranie Nord occidentale. *Thèse Doc. Etat*, U.S.T.H.B, Alger, (1985), 296 p.

Mutlu, H.: Chemical geothermometry and fluid-mineral equilibria for the Omer-Gecek thermal waters, Afyon area, Turkey, J Volcanol Geotherm Res, **80**, (1998), 303-321.

Nieva, D., and Nieva, R.: Development in geothermal energy in Mexico, part 12—a cationic composition geothermometer for prospection of geothermal resources. *Heat Recover Syst,* CHP **7**, (1987), 243–258.

Nocquet, J.M., and Calais, E.: Geodetic measurements of crustal deformation in the western Mediterranean and Europe, *Pure Appl. Geophys*, **161**, (2004), 661-681.

Perrodon, A.: Etude géologique des bassins néogènes sublittoraux de l'Algérie occidentale. *Service de la Carte Géologique de l'Algérie (Nouvelle Série)*, **Bulletin N_ 12**, (1957), 368p.

Rimi, A., Zarhloule, Y., Barkaoui, A.E., Correi, A., Carneiro, J., and Verdoya, M. Towards a de-carbonized energy system in north-eastern Morocco: prospective geothermal resource. *Renew Sustain Energy Rev*, **16**, (2012), 2207-2216.

Rozanski, K., Araguás-Araguás, L., and Gonfiantini, R.: Isotopic patters in modern global precipitation, In: Swart, P.K.: (ed) Climate change in continental isotopic records, *American Geophysical Union Monogr. Ser*, **78**, Washington, DC, USA, (1993), 1-36.

Saibi, H.: Geothermal resources in Algeria. Proceedings in *World Geothermal Congress*, Melbourne, Australia, (2015).

Savelli, C.: Time-space distribution of magmatic activity in the western Mediterranean and peripheral orogens during the past 30 Ma (a stimulus to geodynamic considerations), *Journal of Geodynamics*, **34 (1)**, (2002), 99–126.

Serpelloni, E., Vannucci, G., Pondrelli, S., Argnani, A., Casula, G., and Anzidei, M.: Kinematics of the western Africa Eurasia plate boundary from focal mechanisms and GPS data, *Geophys J Int*, **169**, (2007), 1180-1200.

Truesdell, A.H.: Summary of section III. Geochemical techniques in exploration, *Proceeding 2nd UN symposium on the development and use of geothermal resources*, San Francisco, (1976), 1, liii-lxxix.

Truesdell, A.H., and Fournier, R.O.: Procedure for estimating the temperature of a hot water component in mixed water by using a plot of silica verses enthalpy. *J Res US Geol Survey*, **5**, (1977), 49-52.

Verdeil, P.: Algerian thermalism in its geostructural setting, how hydrogeology has helped in the elucidation of Algeria's deep seated structure, *J Hydrol*, **56**, (1982), 107–117.

White, A.F.: Chemical and Isotopic characteristics of fluids within the Baca Geothermal Reservoir, Valles Caldera, New Mexico, *J Geophys Res*, **91**, (1986), 1855–1866.

Wildi, W.: La chaine tello-rifaine. Structure, stratigraphie et évolution du Trias au Miocène. *Rev Geol Dyn et geogr Phys*, **24**, (1983), 201–297.